Published in : Journal of Materials Chemistry A (2019), vol. 7, issue 16, pp. 9844-9853
doi.org/10.1039/c9ta01564g
Status : Postprint (Author's version)

CO_2-SOURCED POLYCARBONATES AS SOLID ELECTROLYTES FOR ROOM TEMPERATURE OPERATING LITHIUM BATTERIES †

Farid Ouhib ‡[a], Leire Meabe‡[b], Abdelfattah Mahmoud [c], Nicolas Eshraghi [c], Bruno Grignard [a], Jean-Michel Thomassin [a], Abdelhafid Aqil [a],Frederic Boschini [c], Christine Jérôme [a], David Mecerreyes [b], and Christophe Detrembleur [a]

[a] *Centre for Education and Research on Macromolecules, CESAM Research Unit, University of Liege, Sart-Tilman B6a, 13allée du 6 août, B-4000 Liège, Belgium. E-mail: christophe.detrembleur@uliege.be*
[b] *POLYMAT, University of the Basque Country UPV/EHU, Joxe Mari Korta Centre, Avda. Tolosa 72, 20018 Donostia-San Sebastian, Spain. E-mail: david.mecerreyes@ehu.es*
[c] *GREENMAT-LCIS, Chemistry Department, University of Liège, Sart Tilman B6b, 4000 Liège, Belgium*
‡ *Equal contribution.*

† Electronic supplementary information (ESI) available. See DOI:10.1039/c9ta01564g

Abstract

In the last few years, polycarbonates have been identified as alternatives to poly(ethylene oxide) as polymer electrolytes for lithium battery applications. In this work, we show the design of CO_2-sourced polycarbonates for their use in room temperature operating lithium batteries. Novel functional polycarbonates with alternating oxo-carbonate moieties and polyethylene oxide segments are synthesized by the facile room temperature (rt) organocatalyzed polyaddition of CO_2-sourced bis(α-alkylidene carbonate)s (bis-αCCs) with polyethylene oxide diols. The effect of the molar mass of polyethylene oxide on the ionic conductivity and thermal properties of poly(oxo-carbonate)s is investigated. The best candidate shows a low glass transition temperature of –44 °C and a high ionic conductivity of 3.75×10^{-5} S cm^{-1} at rt when loaded with 30 wt% bis(trifluoromethanesulfonyl)imide salt (LiTFSI) without any solvent. An all-solid semi-interpenetrated network polymer electrolyte (SIN-SPE) is then fabricated by UV cross-linking of a mixture containing specifically designed poly(oxo-carbonate) bearing methacrylate pendants, diethylene glycol diacrylate and the previously described poly(oxo-carbonate) containing LiTFSI. The resulting self-standing membrane exhibits a high oxidation stability up to 5 V (vs. Li/Li^+), an ionic conductivity of 1.1×10^{-5} S cm^{-1} at rt (10^{-4} S cm^{-1} at 60 °C) and promising mechanical properties. Assembled in a half cell configuration with $LiFePO_4$ (LFP) as the cathode and lithium as the anode, the all-solid cell delivers a discharge capacity of 161 mA h g^{-1} at 0.1C and 60 °C, which is very close to the theoretical capacity of LFP (170 mA h g^1). Also, a stable reversible cycling capacity over 400 cycles with a high coulombic efficiency of 99% is noted at 1C. Similar results are obtained at rt provided that 10 wt% tetraglyme as a plasticizer was added to the SIN-SPE.

1. Introduction

Today, the development of safe and efficient electrochemical devices for the storage of energy generated by intermittent renewable sources has become a strategic driver for ecological transition.[1,2] As a result of

Published in : Journal of Materials Chemistry A (2019), vol. 7, issue 16, pp. 9844-9853
doi.org/10.1039/c9ta01564g
Status : Postprint (Author's version)

their high specific energy and energy density, Li-ion batteries (LIBs) have emerged as key players for tackling this major challenge.[3,4] However, these devices generally use mixtures of cyclic organic carbonates in combination with lithium salts as liquid electrolytes. These liquids cause some important safety issues such as flammability and the release of toxic products when the battery is damaged.[5] To surpass these hurdles, solid polymer electrolytes (SPEs) doped with a lithium salt are promising alternatives to organic liquid electrolytes[6,7] and are expected to become key structural elements for the next generation of high performance and safe all-solid batteries.[8,9] Ideal SPEs should display specific features such as (1) a good ionic conductivity (>10^{-4} S cm^{-1} at room temperature (rt)) to ensure ion transport and rapid charge/discharge, (2) a Li^+ transference number close to unity in order to reduce the concentration polarization of salts during operation and to produce high power density,[10] (3) suitable mechanical properties for elastic and flexible all-solid batteries that will prevent the formation of metal dendrites responsible for short circuits, and (4) a wide electrochemical stability window (up to 4–5 V *vs*. Li/Li^+) to be compatible with both electrode materials and to prevent their degradation during battery operation.[11,12]

Poly(ethylene oxide) (PEO) mixed with a lithium salt is the most popular SPE used in battery applications.[13,14] The polar ether oxygen atoms of PEO dissociate the salt and Li^+ cations are transported by the segmental motion chains, mainly in the amorphous phase.[15,16] However, the major drawbacks of PEO-based SPEs are their low Li^+ transference number (<0.2), modest ionic conductivity at room temperature (<10^{-5} S cm^{-1}) and narrow electrochemical stability (<4 V *vs*. Li^+/Li).[17] Moreover, their poor mechanical properties resulting from the plasticization of PEO by the dissolved organic salt and their low melting temperature are not sufficient to avoid short circuits between the two electrodes. This limits the battery operation of PEO SPEs to high temperatures (>70 °C and low voltage cathodes). In the quest for high performance SPEs, some research groups have demonstrated the beneficial effect of introducing carbonate moieties within the main PEO chains on the ionic mobility.[18] The large dipole moment of the carbonates improved the salt dissociation and increased the segmental motion ability of the copolymer chains, yielding ionic conductivity values higher than 10^{-5} S cm^{-1} at rt and a Li^+ transference number (0.5) close to unity, indicating the potential for room temperature battery operation. However, these solid electrolytes, synthesized by copolymerization of dimethyl carbonate with poly(ethylene oxide)diol at high temperature (180 °C), are sticky materials that cannot be handled as self-standing membranes for lithium battery applications. The partial decarboxylative ring-opening polymerization of 5-membered cyclic carbonates and the ring-opening copolymerization of CO_2 with epoxides are elegant and facile approaches to design poly(ether-*co*-carbonate)s for potential SPE applications.[19–22] However, the difficulty of introducing functional groups within/along the poly(ether-co-carbonate) backbone is a key issue for tailoring self-standing SPE membranes with appropriate mechanical resistance.

Recently, some of us introduced a novel and versatile route to synthesize functional polycarbonates, poly(β-oxo-carbonate) s, by facile room temperature organocatalyzed polyaddition of CO_2-sourced bis(α-alkylidene carbonate)s (bis-αCCs) with diols.[23] Herein, we exploit this toolbox to synthesize an unprecedented self-standing SPE membrane that is evaluated in a $Li/LiFePO_4$ cell. We demonstrate that poly(β-oxo-carbonate) s with alternating flexible PEO sequences and oxo-carbonate groups present a high ionic conductivity at rt. By adapting the synthetic procedure, we also prepared poly(b-oxo-carbonate) bearing crosslinkable methacrylate pendants in a simple one-pot process. The two polymers are then processed into a semi-interpenetrated polymer network (SIN) with improved mechanical properties and high electrochemical stability. The performances of this SIN in a $Li/LiFePO_4$ cell are evaluated at 60 °C and at rt.

Published in : Journal of Materials Chemistry A (2019), vol. 7, issue 16, pp. 9844-9853
doi.org/10.1039/c9ta01564g
Status : Postprint (Author's version)

2. Experimental section

2.1 Materials and synthetic part

Poly(ethylene glycol) (M_n = 1500 g mol^{-1}), poly(ethylene glycol) (M_n = 2000 g mol^{-1}), poly(ethylene glycol) (M_n = 4000 g mol^{-1}) and diethylene glycol diacrylate (99%) were purchased from Aldrich. 1,8-Diazabicyclo[5.4.0]undec-7-ene (DBU, 99%) was purchased from Fluorochem. Lithium bis(trifluoromethane) sulfonimide (LiTFSI) (99.9%) was supplied by Solvionic and used as received. Meso-4,4-dimethyl-5-methylene-1,3-dioxolan2-one (bis-αCC) was synthesized as reported elsewhere by our group.[18,23] 1,3-Dihydroxy-2-methylpropan-2-yl methacrylate was synthesized as reported in the literature.[24,25]

General synthetic procedure for PEO/poly(b-oxo-carbonate).
In a typical experiment for **PC-1**, 200 mg of bis-αCC (0.787 mmol, 1 eq.) and 1181 mg (0.787 mmol, 1 eq.) of poly(ethylene glycol) (M_n = 1500 g mol^{-1}) were added in a reaction tube with 1.3 mL of dry DMSO. 0.2 mL (0.04 mmol, 0.05 eq.) of DBU solution (*C* = 0.2 M in DMSO) was added and the reaction medium was stirred at 25 °C. After 24 h, the obtained polymer was purified by double precipitation in diethyl ether. The purified polymer was dried under vacuum at 60 °C (1284 mg, 93% yield).

PC-2 and **PC-3** were synthesized with the same procedure. ^{1}H and ^{13}C-NMR spectra are reported in the ESI.†

Synthesis of crosslinkable PC (PC-4): 200 mg of bis-αCC (0.787 mmol, 1 eq.), 68 mg (0.393 mmol) of 1,3-dihydroxy-2methylpropan-2-yl methacrylate and 1574 mg (0.393 mmol, 1 eq.) of poly(ethylene glycol) (M_n = 4000 g mol^{-1}) were added in a reaction tube with 1.8 mL of dry DMSO. 0.2 mL (0.04 mmol, 0.05 eq.) of DBU solution (*C* = 0.2 M in DMSO) was added and the reaction medium was stirred at 25 °C. After 24 h, the obtained polymer was purified by double precipitation in diethyl ether. The purified polymer was dried under vacuum at room temperature (1602 mg, 89% yield).

Preparation of polymer electrolytes
Solid poly(oxo-carbonate) electrolyte. 70 mg of aliphatic poly(β-oxo-carbonate) and 30 mg of LiTFSI were dissolved in 1 mL of acetone. After 1 h of mixing, the solvent was evaporated at room temperature followed by a thermal treatment for 24 h at 60 °C.

All solid cross-linked SPE. 60 mg of **PC-3**, 20 mg of cross-linkable polycarbonate (PC-4), 20 mg of diethylene glycol diacrylate, 42.85 mg of LiTFSI and 3 mg of 2-hydroxy-2-methylpropiophenone (photoinitiator) were dissolved in 1 mL of acetone. After 1 h, the solution was cast onto a silicon mold. The solvent was removed under ambient conditions followed by a high vacuum treatment. Finally, the films were passed 3 times under a xenon arc lamp (Helios Italquartz, 45 mW cm^{-2}). Before performing electrochemical characterization, the SPEs were dried under vacuum at rt for 24 h, followed by increasing the temperature up to 60 °C for 2 h.

2.2 Characterization methods

Nuclear magnetic resonance (NMR) spectroscopy. ^{1}H and ^{13}C NMR analyses were performed on Bruker Avance 250 or 400 MHz spectrometers in $CDCl_3$, DMSO or DMF at 25 °C in the Fourier transform mode. 16 or 64 scans for ^{1}H spectra and 512 or 2048 scans for ^{13}C spectra were recorded.

Published in : Journal of Materials Chemistry A (2019), vol. 7, issue 16, pp. 9844-9853
doi.org/10.1039/c9ta01564g
Status : Postprint (Author's version)

Gel permeation chromatography (GPC). The number-average molecular weight (M_n) and molar-mass dispersity ($Đ$) of the different polymers were determined by size exclusion chromatography (SEC) in THF at 45 °C at a flow rate of 1 mL min^{-1} with a Viscotek 305 TDA liquid chromatograph equipped with two PSS SDV linear M columns calibrated with poly(methyl methacrylate) standards and a refractive index detector.

Differential scanning calorimetry (DSC) was performed on a DSC Q2000 differential calorimeter (TA Instruments). All the experiments were performed under ultrapure nitrogen flow. Samples of 5–8 mg were used. Measurements were performed by placing the samples in sealed aluminium pans. The samples were first heated at a rate of 20 K min^{-1}, from 30 °C to 100 °C and they were left for 3 min at 100 °C to eliminate the thermal history. Subsequently, the samples were cooled down to -70 °C at a rate of 10 K min^{-1} and subsequently heated to 100 °C at 10 K min^{-1} after waiting at -70 °C for 3 min. Once again, the samples were cooled at a rate of 50 K min^{1} until 70 °C, and later they were heated up at 20 K min^{-1} up to 100 °C, in order to determine the glass transition temperature.

Rheological measurements were performed using an ARESG2 rheometer from TA Instruments equipped with an ARESG2 curing accessory, made of a light guide, a quartz plate and a reflecting mirror assembly allowing the transfer of UV radiation from the UV-light source to the sample. UV curing at 365 nm was performed with an OmniCure Series 2000 (200 W, 365 nm). Typically, 60 mg of aliphatic polycarbonate, 20 mg of cross-linkable polycarbonate, 20 mg of diethylene glycol diacrylate, 42.85 mg of LiTFSI and 3 mg of 2-hydroxy-2-methylpropiophenone (ultraviolet initiator) were dissolved in 1 mL acetone. After stirring for 1 h, the solutions were casted onto the rheometer plate (disc of 2 cm in diameter). The acetone was evaporated under ambient atmosphere for 30 min, and then under vacuum for 10 min. The time evolutions of the elastic and viscous moduli were recorded at a frequency of 1 Hz and a strain of 1% without and under UV irradiation at 365 nm. Stress–strain experiments were performed with an Instron 5566 at r.t. The membrane was positioned in between the two clamps of the machine and a deformation rate of 2 mm min^{-1} was applied until the sample broke.

X-ray diffraction (XRD). The prepared SPE membranes (**SINPC-3** and **SIN-PC-3/TEG**) were characterized by X-ray diffraction (XRD) using a Bruker D8 diffractometer (Cu Kα radiation) in the range of 10–90°.

The ionic conductivity was studied by electrochemical AC impedance spectroscopy (EIS) with an Autolab 302N potentiostat galvanostat with temperature controlled by a Microcell HC station. The membranes were placed between two stainless steel electrodes and sealed in a Microcell under an inert atmosphere in a glove box (M-Braun) to avoid the contact of the sample with moisture. The frequency range was set from 0.1 MHz to 0.1 Hz and the amplitude was 10 mV. In all the cases the average surface area of the electrode was 0.5026 cm^2. The lithium transference number and electrochemical stability of the SPE were characterized in coin cells CR2032, and the values were measured using Autolab 302N potentiostat galvanostat. For the lithium transference number the SPE was sandwiched between two lithium disks, whereas for electrochemical stability it was sandwiched between a lithium disk and a stainless steel (SS) electrode. Before the analysis, the coin cells were le to stabilize at 70 °C for 24 h. The lithium transference number was calculated based on the Bruce and Vincent method at 70 °C. The electrochemical stability window was determined from the cyclic voltammogram (CV) of the polymer electrolyte at 70 °C. The anodic limit was evaluated between the open circuit potential (OCV) and 5.5 V *vs*. Li^+/Li at a constant rate of 0.5 mV s^{-1}.

The battery performances of the electrolyte membranes were analyzed in two-electrode coin cells, using C-coated $LiFePO_4$ (LFP) provided by Prayon-beLife company (Pholicat FE-100) as the working electrode, Li

Published in : Journal of Materials Chemistry A (2019), vol. 7, issue 16, pp. 9844-9853
doi.org/10.1039/c9ta01564g
Status : Postprint (Author's version)

metal (Aldrich), and solid cross-linked or plasticized SPE (**SIN-PC-3** and **SIN-PC-3/TEG**) as the solid electrolyte. The positive electrode was prepared by dispersing 60 wt% $LiFePO_4$, 20 wt% conductive carbon (Super P), and 20 wt% poly(β-oxo-carbonate) **PC-3** as the binder in acetone under stirring for 2 h. The resulting slurry was coated on aluminum foil using the doctor-blade method with a thickness of 120 mm and then dried at 50 °C in a vacuum for 8 h. Discs of 1.2 cm diameter, containing 1–2 mg cm^{-2} of $LiFePO_4$ were cut. For the preparation of all-solid cross-linked SPEs (**SIN-PC-3**), 600 mg of **PC-3**, 200 mg of cross-linkable polycarbonate **PC-4**, 200 mg of diethylene glycol diacrylate, 420 mg of LiTFSI and 30 mg of 2-hydroxy-2-methylpropiophenone (photoinitiator) were dissolved in 2 mL of acetone. After 1 h, the solution was cast onto a Teflon mold. The acetone was removed under ambient conditions followed by a high vacuum treatment. Finally, the films were passed 3 times under a xenon arc lamp (Helios Italquartz, 45 mW cm^{-2}). Before battery assembly, the SPEs were dried under vacuum at rt for 24 h. Discs of 1.4 cm diameter (~100 µm thickness) were cut. Cross-linked SPEs, **SINPC-3**, with TEG were prepared according to the same procedure and by adding 120 mg of tetraglyme to a mixture of 600 mg of **PC-3**, 200 mg of cross-linkable polycarbonate **PC-4**, 200 mg of diethylene glycol diacrylate, 420 mg of LiTFSI and 30 mg of 2hydroxy-2-methylpropiophenone. The **SIN-PC-3** based electrolyte was sandwiched between metallic lithium and the working electrode. CR2032 coin cells were assembled under argon in a glove box. The galvanostatic charge/discharge curves were recorded using a multichannel Biologic potentiostat (VMP3) between 2.5 and 4.2 V *vs*. Li^+/Li^0 at different cycling rates C/*n* (1 Li per f.u. in *n* hours). Cycling galvanostatic measurements were conducted under thermostatic conditions at 25 ± 0.5 and at 60 ± 1 °C. For the rate capability, the cells were cycled at charge/ discharge rates from 0.1 to 1C. After the rate capability study, the cells were cycled back at a lower rate (0.5C) for 4 cycles to test if the reduction of capacity at the highest rates is reversible, which gives an indication of the stability of the electrolyte polymer at high current densities. All over the manuscript, the capacity is referenced to the mass of $LiFePO_4$ in the composite cathode.

3. Results and discussion

3.1 Synthesis and characterization of poly(oxo-carbonate)s

As illustrated in Scheme 1, three poly(oxo-carbonate)s were synthesized by DBU organocatalysed polyaddition of bis-αCC with PEO diol of various molar masses (1500, 2000 and 4000 g mol^{-1}) at rt in DMSO. The structures of the regioregular poly(oxo-carbonate)s, denoted as **PC-1** (prepared from PEO 1500 g mol^{-1}), **PC-2** (prepared from PEO 2000 g mol^{-1}) and **PC-3** (prepared from PEO 4000 g mol^{-1}), were confirmed by ^1H- and ^{13}C-NMR spectroscopy (Fig. S1 and S2†).

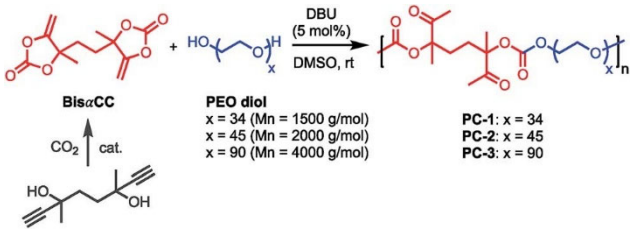

Scheme 1 Reaction scheme for poly(oxo-carbonate)s.

^1H-NMR spectra of the three polymers show the characteristic peaks of the methylene proton adjacent to the carbonate groups at 4.2 ppm and the peak of the methyl in the α position of the ketone groups at 2.15

Published in : Journal of Materials Chemistry A (2019), vol. 7, issue 16, pp. 9844-9853
doi.org/10.1039/c9ta01564g
Status : Postprint (Author's version)

ppm. The apparent molar masses (M_n) of the purified copolymers were determined by size exclusion chromatography (SEC) with THF as the eluent and by using PEO standards. All polymers showed high M_n values of 45 000 to 60 000 g mol^{-1} and molar-mass dispersities ($Đ$) of 1.5– 1.6. All macromolecular characteristics of the polymers, as well as their thermal properties, are summarized in Table 1.

The thermal properties of the three copolymers (Fig. S3†), evaluated by DSC, showed a semi-crystalline behavior with a melting temperature (T_m) of 23 °C for **PC-1** that increased up to 41 °C for **PC-3** (Table 1). All copolymers exhibited a low glass transition temperature (T_g) that decreased from -43 °C for **PC-1** to -52 °C for **PC-2** and **PC-3**. These thermal properties are mainly dictated by the molar mass of PEO introduced within the copolymer chain.

Table 1 Molecular characteristics and thermal properties of poly(oxo-carbonate)s

Entry	M_n of PEO (g mol^{-1})	M_n (g mol^{-1})	$Đ$	T_g (°C)	T_m (°C)	ΔH_f (J g^{-1})
PC-1	1500	60 000	1.66	-43	23	56
PC-2	2000	45 000	1.55	-52	31	60
PC-3	4000	49 000	1.53	-52	41	67

3.2 Evaluation of poly(oxo-carbonate)s as solid polymer electrolytes (SPEs)

Several studies with other polyether polycarbonates and polyester polycarbonates showed that a 30–36 wt% LiTFSI composition provided the highest ionic conductivity value.[18,26–28] We therefore decided to include 30 wt% LiTFSI in the formulation. We thus prepared SPEs by mixing the different polymers (**PC-1**–3) with 30 wt% LiTFSI in acetone, followed by solvent removal.

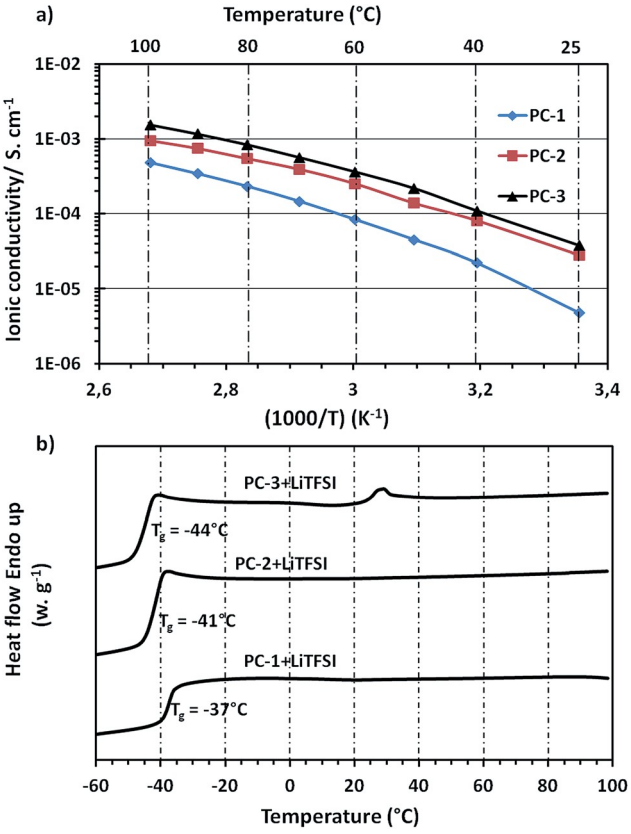

Fig. 1 (a) Arrhenius plot, temperature dependence of the ionic conductivity, and (b) DSC traces for the second heating of **PC-1**, **PC-2** and **PC-3** containing 30 wt% LiTFSI.

Published in : Journal of Materials Chemistry A (2019), vol. 7, issue 16, pp. 9844-9853
doi.org/10.1039/c9ta01564g
Status : Postprint (Author's version)

The thermal properties of the three SPEs and their anhydrous ionic conductivities were evaluated by dynamic scanning calorimetry (DSC) and electrochemical impedance spectroscopy (EIS), respectively. The ionic conductivity of the three SPEs was evaluated at temperatures ranging from 100 °C to 25 °C. The results are depicted in Fig. 1a and show a clear increase of the ionic conductivity with the molar mass of PEO incorporated within the PC chain. These results indicate that a higher number of ethylene oxide units increases the segmental motion, which favors the ionic mobility. At 25 °C, an ionic conductivity of 3.75 × 10^{-5} S cm^{-1} was measured for **PC-3** which is 7.8 times higher than that obtained for **PC-1** (4.86 × 10^{-6} S cm^{-1}). The ionic conductivity of **PC-3** (3.75 × 10^{-5} S cm^{-1} at room temperature and 1.86 × 10^{-4} S cm^{-1} at 60 °C) is comparable to or even better than those determined for the most efficient polycarbonate-based SPEs.[18,27,29–33]

DSC curves of the three SPEs are shown in Fig. 1b. All PCs were plasticized with LiTFSI, resulting in SPEs with suppressed or decreased melting temperature. The introduction of LiTFSI prevents the crystal formation and the materials result in amorphous SPEs. In **PC-3**, a small melting enthalpy can be observed at 30 °C. However, the ionic conductivity of **PC-3** does not seem to be affected by the crystallinity. The glass transition temperature has a bigger effect on the ionic conductivity. The T_g of SPEs decreased with the molar mass of PEO, from -37 °C for **PC-1** to -41 °C for **PC-2** and to -44 °C for **PC-3**.

This result is in agreement with the highest ionic conductivity observed for **PC-3**. Despite its attractive ionic conductivity, the **PC-3** based SPE was however a sticky material that could not form a self-standing membrane.

3.3 Preparation and characterization of self-standing SPE membranes

In order to improve the mechanical properties of the SPEs, we prepared a semi-interpenetrated network (SIN) *via* photochemical crosslinking of a novel poly(oxo-carbonate) bearing methacrylate pendant (**PC-4**) with diethylene glycol diacrylate, in the presence of **PC-3**, LiTFSI, and 2-hydroxy-2methylpropiophenone as the photo-initiator (Scheme 2).

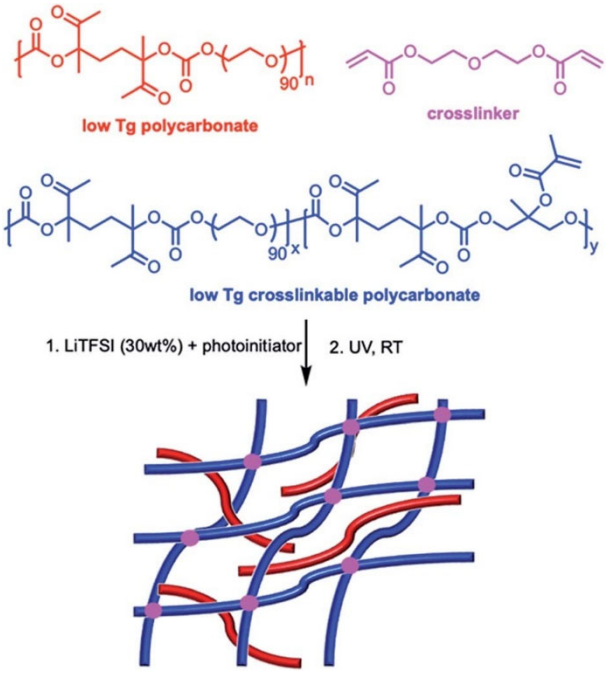

Scheme 2 General strategy for the design of solid semi-interpenetrated polymer electrolytes from poly(β-oxo-carbonate)s.

Published in : Journal of Materials Chemistry A (2019), vol. 7, issue 16, pp. 9844-9853
doi.org/10.1039/c9ta01564g
Status : Postprint (Author's version)

The cross-linkable poly(oxo-carbonate) **PC-4** was designed to mimic **PC-3** that presented the highest ionic conductivity. It was prepared by the DBU organocatalysed polyaddition of bis-αCC with a mixture of two diols, PEO diol (M_n = 4000 g mol^{-1}) and 1,3-dihydroxy-2-methylpropan-2-yl methacrylate (DHMPM), at rt in DMSO (Scheme 3). DHMPM was synthesized following the work of L. I. Ronco et al.[25] After 24 h of reaction, **PC-4** was collected with 89% yield with a M_n of 28 000 g mol^{-1} and a molar-mass dispersity of 1.5. Fig. S4† shows the ^{1}H-NMR spectrum of the copolymer that confirms the copolymer structure and the incorporation of 48 mol% methacrylate moieties into the polymer chains. The photopolymerization of diethylene glycol diacrylate and methacrylate pendant groups was verified by Fourier transform infrared spectra by the complete disappearance of the bands associated with the C=C double bonds of acrylates and methacrylates at 1600–1650 cm^{-1} after crosslinking (Fig. S5†).

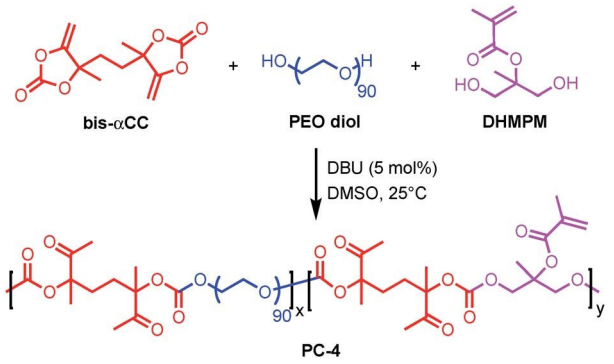

Scheme 3 Reaction scheme for crosslinkable poly(oxo-carbonate) PC-4.

The cross-linking reaction for the formation of SIN-SPEs was then followed by rheology experiments (Fig. 2a) on the following formulation: **PC-3** (41.4 wt%), LiTFSI (29 wt%), **PC-4** (13.8 wt%), diethylglycol diacrylate (13.8 wt%) and the photoinitiator (2 wt%). The elastic (*G*') and loss (*G*'') moduli of the SIN-SPE, named **SIN-PC-3**, were measured as a function of time for 200 s in the dark, followed by 200 s under UV-irradiation at 365 nm at rt. In the absence of UV light, the loss modulus (*G*'') is higher than the elastic modulus (*G*') as expected for a non-crosslinked polymer (Fig. 2a). Upon exposure to UV light, both moduli drastically increased after a few seconds of reaction, with *G*' increasing more rapidly (from 0.6 to 9.9 MPa) than *G*'' (from 0.8 to 2.3 MPa). The cross-over point that was observed after about 20 s corresponds to the network formation, with *G*' values becoming higher than *G*''. A self-standing transparent membrane was collected after a few seconds of irradiation (Fig. 2c).

This self-standing membrane presents enhanced mechanical properties compared to the **PC-3**/LiTFSI SPE with the same LiTFSI content (30 wt%) with a *G*' value as high as 8.5 MPa for **SIN-PC-3** vs. 0.06 × 10^{-8} MPa for **PC-3** at 0.01 rad s^{-1}, Fig. S6.†

Published in : Journal of Materials Chemistry A (2019), vol. 7, issue 16, pp. 9844-9853
doi.org/10.1039/c9ta01564g
Status : Postprint (Author's version)

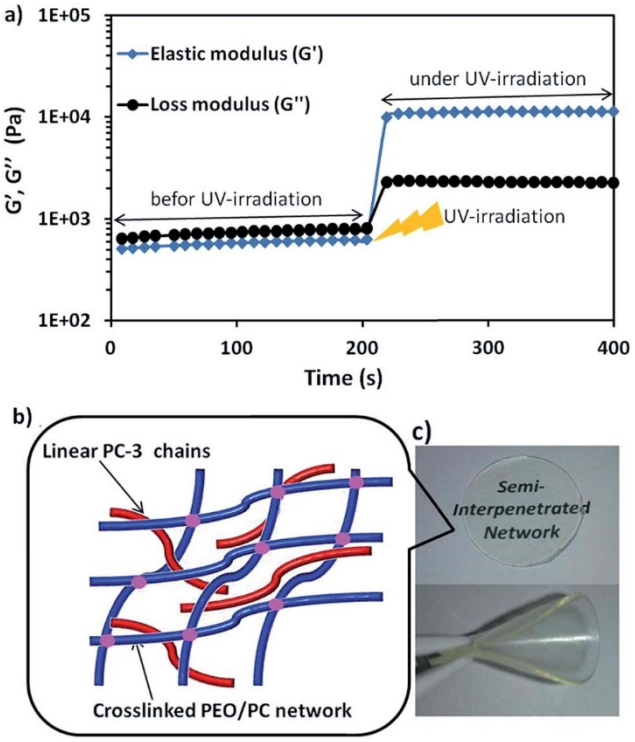

Fig. 2 (a) Elastic (*G*') and loss (*G*'') moduli of **SIN-PC-3** before and after UV crosslinking; (b) schematic representation and (c) picture of the self-standing **SIN-PC-3** membrane.

Stress/strain experiments were then performed on **SIN-PC-3** in order to evaluate its mechanical properties at room temperature. This experiment enabled the determination of its Young's modulus (E = 13 ± 2.1 MPa), elongation at break (ε_{break} = 33 ± 4%) and stress at break (σ = 1.1 ± 0.2 MPa) (Fig. S6b and Table S1†). These values are in the range of values generally recognized as suitable for the application of **SIN-PC-3** as a solid electrolyte.[34–36] Conclusively, **SIN-PC-3** presents appropriate mechanical properties and elasticity for the design of flexible solid electrolytes. It is expected to maintain good interfacial contact and to prevent the formation of lithium dendrites in lithium ions batteries.[36,37] The dimensional stability of the **SIN-PC-3** membrane was also evaluated at rt and 100 °C. After 1 h at 100 °C, only a negligible increase (2%) of the dimensions of the membrane was noted compared to that at rt (Fig. S7†), attesting to the excellent dimensional stability of the membrane over a large temperature range (25 °C to 100 °C).

The thermal properties and temperature dependence of the ionic conductivity of **SIN-PC-3** were then measured under similar conditions to those used for the **PC-3** based SPE (containing 30 wt% LiTFSI). As presented in Fig. 3a, the ionic conductivity of **SIN-PC-3** (1.11×10^{-5} S cm^{-1} at rt) was slightly lower than that measured for the **PC-3** based SPE (3.75×10^{-5} S cm^{-1} at rt), whereas T_g was only slightly affected (-42 °C for **SIN-PC-3** *vs*. -44 °C for **PC-3** SPE; Fig. 3b) by the formation of the cross-linked network. This three-dimensional system limits the chain mobility and causes a slight decrease in ionic conductivity with respect to **PC-3**. X-ray diffraction (XRD) was then performed on the **SIN-PC-3** membrane. In contrast to PEG that presents intense and narrow peaks,[38] the diffractogram of **SIN-PC-3** shows two broad peaks, in line with the absence of highly ordered crystallinity and the amorphous nature of the membrane (Fig. S8†).

The lithium transference number (t_{Li+}) is used to describe the Li^+ ion transfer ability of the SPEs, which is related to the rate capability of Li^+ in the electrolyte. It is accepted that carbonyl groups are able to dissociate the lithium cation from the TFSI anion.[18,39,40] Therefore, they will promote lithium conduction. In

Published in : Journal of Materials Chemistry A (2019), vol. 7, issue 16, pp. 9844-9853
doi.org/10.1039/c9ta01564g
Status : Postprint (Author's version)

order to demonstrate this, the cation transference number (t_{Li+}) calculated using the Bruce and Vincent method at 70 °C was t_{Li+} = 0.28 for **SIN-PC-3** (Fig. S9†), which is improved with respect to the reported value for PEO (t_{Li+} = 0.20). [13,41] This result is consistent considering the relation between ethylene oxide units and carbonate groups that we have in the polymer, even though the effect of the carbonyl group is not as effective as it is in other polycarbonate based SPEs.[18,39,40] Additionally, FTIR-ATR was used to confirm the coordination of lithium cations with carbonyl groups. A slight coordination of lithium with carbonyl groups is detected from the analysis, which is the reason for the improvement of the t_{Li+} value, Fig. S10.†

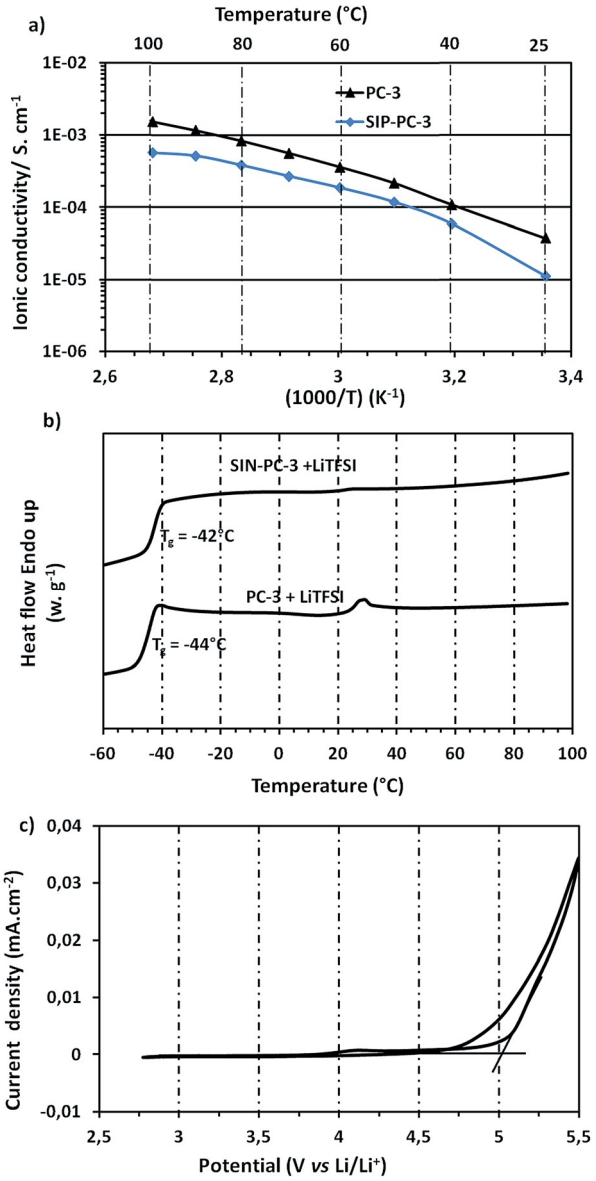

Fig. 3 (a) Arrhenius plot, temperature dependence of ionic conductivity, (b) DSC traces for the second heating of solid electrolyte based **SIN-PC-3** and **PC-3**, and (c) electrochemical stability window of the **SIN-PC-3** SPE obtained by CV at a scan rate of 0.5 mV s^{-1}.

The electrochemical stability window of **SIN-PC-3** was investigated by cyclic voltammetry (CV) at 70 °C. As shown in Fig. 3c, **SIN-PC-3** was stable up to 5 V (*vs*. Li^+/Li), demonstrating an enhanced electrochemical stability of our electrolyte compared to PEO-based SPEs reported in the literature.[13,42] Consequently, **SIN-PC-3** appeared as a promising SPE candidate for Li batteries with highly positive active materials.

Published in : Journal of Materials Chemistry A (2019), vol. 7, issue 16, pp. 9844-9853
doi.org/10.1039/c9ta01564g
Status : Postprint (Author's version)

3.4 Electrochemical performances of the all-solid state lithium battery

We then evaluated the polycarbonate-based semi-interpenetrated network SPE in an all-solid-state lithium battery. For this purpose, we fabricated a prototype half-cell by sandwiching **SIN-PC-3** between lithium metal as the anode and lithium iron phosphate ($LiFePO_4$, LFP) as the cathode, without any additional separator.

Fig. 4a and b present the charge–discharge profile and rate performances of the Li/**SIN-PC-3**/LFP cell obtained at various rates, increased stepwise from 0.1 to 1C and returned to 0.5C at 60 °C. The analysis of the curves shows that the capacity does not decay significantly on increasing the C-rate. The working voltage decreases mainly at a high C-rate; however the discharge and charge plateaus almost keep their □at shape for all rates. The cell delivered a discharge capacity of 161 mA h g^{-1} at 0.1C which is very close to the theoretical capacity of LFP (170 mA h g^{-1}). The charge/discharge capacity did not drop much on increasing the C-rate. It was even possible to cycle at a C-rate of 1C with a good discharge capacity of 102 mA h g^{-1}. When the current returned to 0.5C, the discharge capacity was back to 127 mA h g^{-1}, indicating good stability and reversibility of the **SIN-PC**-3 solid electrolyte even after cycling under high current densities. It is worth noting that there is a short pseudo-plateau that appears in the charge curves of the **SIN-PC-3**/Li/$LiFePO_4$ cell at around 4.0 V, as shown in Fig. 4a, especially for C/2 and C/5. We did not observe this plateau for the cycling rate of C/10 and 1C at 60 °C, and also during cycling at RT for all rates (see later discussion of Fig. 5). The origin of this plateau is not understood yet; however the reaction that is responsible for this observation does not affect the electrochemical performance of the **SIN-PC-3**/Li/$LiFePO_4$ cell at 60 °C, even under relatively higher charge/discharge C-rates (C/2, 1C) (see below the discussion related to the long cycling performance of the cell). Fig. 4c illustrates the long cycling performance of the cell at a current density of 170 mA g^{-1} (1C) at 60 °C. The cell delivered a first charge capacity of 99 mA h g^{-1}, and the discharge capacity was 97 mA h g^{-1}. This irreversible capacity during the first cycle might be related to the formation of a surface film at the cathode polymer electrolyte interface and other side reactions. From the second cycle, the coulombic efficiency was maintained at a constant value of 100%. After 400 cycles, the reversible capacity was still as high as 83 mA h g^{-1}, corresponding to about 86% of its initial capacity. This result confirms the long cycle life of the cell, and thus the good electrochemical stability of the poly(oxo-carbonate)-based solid electrolyte even at high temperature (60 °C). Compared to other crosslinked polycarbonate or polyether based SPEs, **SIN-PC-3** exhibits competitive battery performances and stability at 60 °C.[29,31,32,43–48]

The same cell was however not cycled at rt. Indeed, the ionic conductivity of **SIN-PC-3** is not high enough for practical battery applications at this temperature. One of the most popular approaches to improve the ionic conductivity of SPEs consists of adding molecular plasticizers such as succinonitrile or low molecular weight PEG with methoxy end-groups.[49,50] Most studies report that large amounts of plasticizers (20–70 wt%) were required to significantly increase the ionic conductivity. However, these plasticizers negatively affected the mechanical properties of the membrane and liquid leakage was also a risk during operation.[35]

Published in : Journal of Materials Chemistry A (2019), vol. 7, issue 16, pp. 9844-9853
doi.org/10.1039/c9ta01564g
Status : Postprint (Author's version)

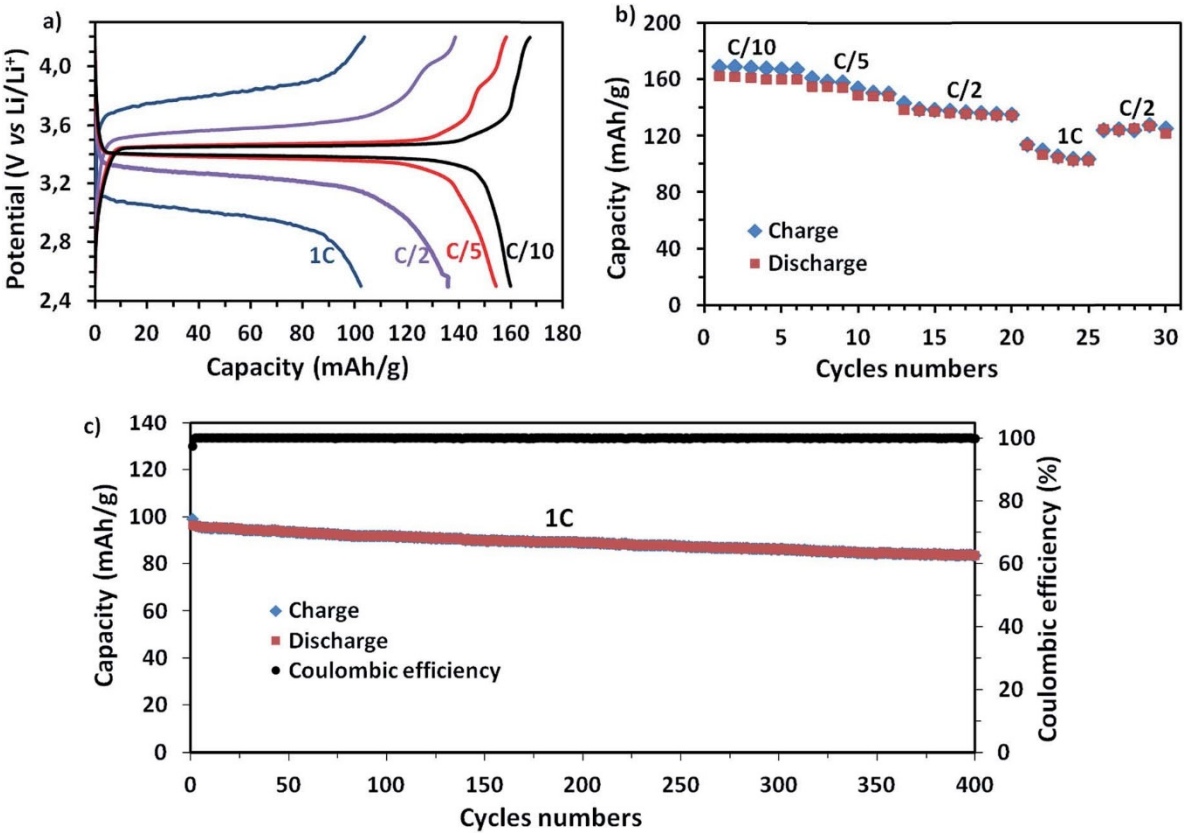

Fig. 4 Electrochemical performances of the all-solid **SIN-PC-3**/Li/$LiFePO_4$ cell in the voltage range of 2.5–4.2 V at 60 °C. (a) Charge–discharge profiles, (b) the reversible capacity at various current rates (C/10 to 1C) and (c) cycle performance of the cell at a current rate of 1C.

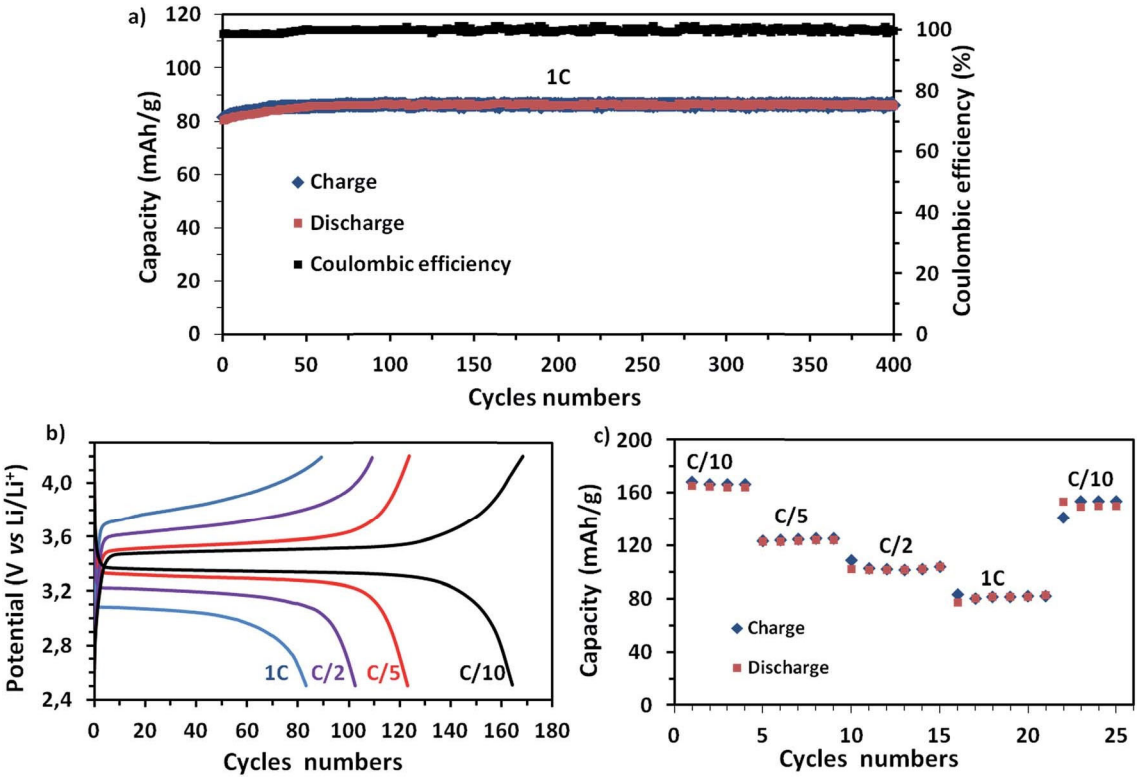

Fig. 5 Electrochemical performances of the batteries based on the **SIP-PC-3**/TEG electrolyte at 25 °C (10 wt% TEG). (a) Cycle performance of the Li/$LiFePO_4$ cell at a current rate of 1C; (b) charge–discharge profiles in the potential range from 2.5 to 4.2 V, and (c) the reversible capacity at various current rates (C/10 to 1C).

Published in : Journal of Materials Chemistry A (2019), vol. 7, issue 16, pp. 9844-9853
doi.org/10.1039/c9ta01564g
Status : Postprint (Author's version)

By adding a small quantity of tetraglyme (TEG) as a high boiling point and non-flammable additive (10 wt% vs. the all solid polymer) to **SIN-PC-3**, we enhanced the ionic conductivity of our self-standing membrane at rt (4.7×10^{-5} S cm^{-1} vs. 1.11×10^{-5} S cm^{-1} at rt, Fig. S11†) with no significant effect on the XRD diffractogram of the membrane (Fig. S8†). Only a slight decrease of the mechanical properties of the membrane is noted in the presence of TEG (Fig. S12 and Table S1†). The Young's modulus for the **SIN-PC-3/TEG** membrane remained at an appreciable value of 7.7 ± 0.5 MPa at r.t, which is sufficient to avoid short circuits and improve the safety of LIB devices.[33] The elongation at break decreased to 18% (compared to 33% without TEG), and the stress at break slightly reduced to 0.8 MPa (compared to 1.1 MPa without TEG). The amorphous properties of the **SIN-PC-3/TEG** membrane were verified by XRD analysis (Fig. S8†). Furthermore, the **SIN-PC-3/TEG** membrane is electrochemically stable up to 5 V vs. Li^+/Li (Fig. S13†).

Assembled in a half-cell configuration, excellent cycling performances were achieved for the cell with a discharge capacity of 86 mA h g^{-1} at 1C after 400 cycles at rt (Fig. 5a). The cell exhibited excellent rate capabilities from C/10 to 1C, with a reversible capacity of 165 mA h g^{-1} at C/10 (corresponding to 97% of the theoretical capacity of LFP) and 82 mA h g^{-1} at 1C (48% of the theoretical capacity of LFP) (Fig. 5b and c). The slope of the discharge plateau does not change with the increase of C-rate; the discharge/charge plateau maintains its flat shape at different current densities, and only the working voltage decays slightly with the increase of C-rate which is due to the increase in polarization of the battery mainly at high C-rates.[51,52] These excellent electrochemical performances are the result of TEG that plasticizes **SIN-PC-3**, consequently increasing the mobility of the polymer chains and facilitating lithium ion diffusion.[53,54] This cell containing only 10 wt% TEG presents comparable battery performances to similar cells prepared from SPEs containing higher amounts of plasticizers (20–70%).[36,47,55–58]

Additionally, when compared to other batteries containing carbonate groups in the SPE, we can clearly observe the improvement and advantages of capacity and C-rates provided by the polymer electrolyte that we developed in this work.[20,26,27,59]

4. Conclusions

In this work, new innovative CO_2-sourced polycarbonates were synthesized and optimized as solid electrolytes for room temperature operating lithium batteries. Using these polymers, the electrochemical performance of conventional PEO-SPEs has been improved by the incorporation of a few carbonyl groups. The functional polycarbonates have been synthesized by organocatalyzed polyaddition of CO_2-sourced bis(α-alkylidene carbonate)s (bis-αCCs) with polyethylene oxide diols at room temperature. After analyzing all the polycarbonates designed, the mechanical properties of the best candidate were improved. The SPE with the highest number of ethylene oxide units presented the most valuable electrochemical properties. After analyzing the ionic conductivity (10^{-4} S cm^{-1} at 60 °C), lithium transference number (0.28) and electrochemical stability (5 V), the battery performance was evaluated at 60 °C with LFP as a cathode. The SPE shows a capacity of 83 mA h g^{-1} even after cycling the battery at a C-rate of 1C at 60 °C. These promising results lead to including 10 wt% tetraglyme in the formulation of the SPE with the final goal of cycling the battery at room temperature. All in all, this work corroborates the potential of polycarbonates as solid polymer electrolytes for batteries and highlights the potential of an emerging class of CO_2-sourced monomers and polymers[23,60] for this important application.

Conflicts of interest

There are no conflicts to declare.

Acknowledgements

C. D. thanks the "Fonds National pour la Recherche Scientifique" (F.R.S.-FNRS) and the Fonds Wetenschappelijk Onderzoek – Vlaanderen (FWO) for financial support in the frame of the EOS project no. 019618F (ID EOS: 30902231). The authors from Liege thank the CESAM Research Unit for financial support. C. D. is an F.R.S.-FNRS Research Director. The authors from San Sebastian are grateful for the Financial support of the European Research Council by Starting Grant Innovative Polymers for Energy Storage (iPes) 306250 and the Basque Government through ETORTEK Energigune 2013 and IT 999-16. Leire Meabe thanks the Spanish Ministry of Education, Culture and Sport for the predoctoral FPU fellowship received to carry out this work. The authors are grateful for technical and human support provided by SGIker of UPV/EHU for the NMR facilities of Gipuzkoa campus. A. M. and F. B. are grateful to the Walloon region for a Beware Fellowship Academia 2015-1, RESIBAT no. 1510399 and the support under the "PE PlanMarshall2.vert" program (BATWAL – 1318146).

Notes and references

1 J. Tollefson, *Nature*, 2008, 456, 436–440.

2 M. Armand and J.-M. Tarascon, *Nature*, 2008, 451, 652.

3 J. M. Tarascon and M. Armand, *Nature*, 2001, 414, 359–367.

4 M. Li, J. Lu, Z. Chen and K. Amine, *Adv. Mater.*, 2018, 1800561, 1800561.

5 W. Xu, J. Wang, F. Ding, X. Chen, E. Nasybulin, Y. Zhang and J.-G. Zhang, *Energy Environ. Sci.*, 2014, 7, 513–537.

6 M. Armand, F. Endres, D. R. MacFarlane, H. Ohno and B. Scrosati, *Nat. Mater.*, 2009, 8, 621.

7 W. H. Meyer, *Adv. Mater.*, 1998, 439–448.

8 P. Arora and Z. Zhang, *Chem. Rev.*, 2004, 104, 4419–4462.

9 H. Zhang, C. Li, M. Piszcz, E. Coya, T. Rojo, L. M. Rodriguez-Martinez, M. Armand and Z. Zhou, *Chem. Soc. Rev.*, 2017, 46, 797–815.

10 J. Y. Song, Y. Y. Wang and C. C. Wan, *J. Power Sources*, 1999, 77, 183–197.

11 C. Poinsignon, J. Mater. Sci. Eng. B, 1989, 3, 31–37. 12 F. Croce, G. B. Appetecchi, L. Persi and B. Scrosati, *Nature*, 1998, 394, 456.

13 Z. Xue, D. He and X. Xie, *J. Mater. Chem. A*, 2015, 3, 19218– 19253.

14 L. Y. Yang, D. X. Wei, M. Xu, Y. F. Yao and Q. Chen, *Angew. Chem., Int. Ed.*, 2014, 53, 3631–3635.

15 E. Quartarone and P. Mustarelli, *Chem. Soc. Rev.*, 2011, 40, 2525–2540.

16 J. Yuan, D. Mecerreyes and M. Antonietti, *Prog. Polym. Sci.*, 2013, 38, 1009–1036.

17 J. Kalhoff, G. G. Eshetu, D. Bresser and S. Passerini, *ChemSusChem*, 2015, 8, 2154–2175.

18 L. Meabe, T. V. Huynh, N. Lago, H. Sardon, C. Li, L. A. O'Dell, M. Armand, M. Forsyth and D. Mecerreyes, *Electrochim. Acta*, 2018, 264, 367–375.

19 M. Nakamura and Y. Tominaga, *Electrochim. Acta*, 2011, 57, 36–39.

20 Y. Tominaga, *Polym. J.*, 2016, 49, 291.

21 Y. Tominaga, T. Shimomura and M. Nakamura, *Polymer*, 2010, 51, 4295–4298.

22 M. D. Konieczynska, X. Lin, H. Zhang and M. W. Grinstaff, *ACS Macro Lett.*, 2015, 4, 533–537.

23 S. Gennen, B. Grignard, T. Tassaing, C. Jérôme and C. Detrembleur, *Angew. Chem.*, 2017, 129, 10530–10534.

24 W. Chen, H. Yang, R. Wang, R. Cheng, F. Meng, W. Wei and Z. Zhong, *Macromolecules*, 2010, 43, 201–207.

25 L. I. Ronco, A. Basterretxea, D. Mantione, R. H. Aguirresarobe, R. J. Minari, L. M. Gugliotta, D. Mecerreyes and H. Sardon, *Polymer*, 2017, 122, 117–124.

26 J. Mindemark, B. Sun, E. Törmä and D. Brandell, *J. Power Sources*, 2015, 298, 166–170.

27 W. He, Z. Cui, X. Liu, Y. Cui, J. Chai, X. Zhou, Z. Liu and G. Cui, *Electrochim. Acta*, 2017, 225, 151–159.

28 L. Meabe, N. Lago, L. Rubatat, C. Li, A. J. Müller, H. Sardon, M. Armand and D. Mecerreyes, *Electrochim. Acta*, 2017, 237, 259–266.

29 J. Chai, Z. Liu, J. Ma, J. Wang, X. Liu, H. Liu, J. Zhang, G. Cui and L. Chen, *Adv. Sci.*, 2017, 4, 1600377.

30 Y. Tominaga and K. Yamazaki, *Chem. Commun.*, 2014, 50, 4448–4450.

31 J. Bao, G. Shi, C. Tao, C. Wang, C. Zhu, L. Cheng, G. Qian and C. Chen, *J. Power Sources*, 2018, 389, 84–92.

32 X. Liu, G. Ding, X. Zhou, S. Li, W. He, J. Chai, C. Pang, Z. Liu and G. Cui, *J. Mater. Chem. A*, 2017, 5, 11124–11130.

33 K. Deng, S. Wang, S. Ren, D. Han, M. Xiao and Y. Meng, *ACS Appl. Mater. Interfaces*, 2016, 8, 33642–33648.

34 Q. Pan, D. M. Smith, H. Qi, S. Wang and C. Y. Li, *Adv. Mater.*, 2015, 27, 5995–6001.

35 L. Long, S. Wang, M. Xiao and Y. Meng, *J. Mater. Chem. A*, 2016, 4, 10038–10069.

36 D. G. Mackanic, W. Michaels, M. Lee, D. Feng, J. Lopez, J. Qin, Y. Cui and Z. Bao, *Adv. Energy Mater.*, 2018, 8, 1800703.

37 F. Boujioui, F. Zhuge, H. Damerow, M. Wehbi, B. Améduri and J.-F. Gohy, *J. Mater. Chem. A*, 2018, 6, 8514–8522.

38 Z. Lin, X. Guo and H. Yu, Nano Energy, 2017, 41, 646–653. 39 K. Kimura, J. Motomatsu and Y. Tominaga, *J. Phys. Chem. C*, 2016, 120, 12385–12391.

40 J. Mindemark, L. Imholt, J. Montero and D. Brandell, *J. Polym. Sci., Part A: Polym. Chem.*, 2016, 54, 2128–2135.

41 M. Armand, *Solid State Ionics*, 1983, 9–10, 745–754.

42 S. Sylla, J.-Y. Sanchez and M. Armand, *Electrochim. Acta*, 1992, 37, 1699–1701.

43 Y. Tong, H. Lyu, Y. Xu, B. Prasad Thapaliya, P. Li, X.-G. Sun and S. Dai, *J. Mater. Chem. A,* 2018, 6, 14847–14855.

44 H.-J. Ha, E.-H. Kil, Y. H. Kwon, J. Y. Kim, C. K. Lee and S.-Y. Lee, *Energy Environ. Sci.*, 2012, 5, 6491–6499.

45 J. R. Nair, M. Destro, F. Bella, G. B. Appetecchi and C. Gerbaldi, *J. Power Sources*, 2016, 306, 258–267.

46 H. Ben youcef, O. Garcia-Calvo, N. Lago, S. Devaraj and M. Armand, *Electrochim. Acta*, 2016, 220, 587–594.

47 J. Suk, Y. H. Lee, D. Y. Kim, D. W. Kim, S. Y. Cho, J. M. Kim and Y. Kang, *J. Power Sources*, 2016, 334, 154–161.

48 J. Zhang, J. Yang, T. Dong, M. Zhang, J. Chai, S. Dong, T. Wu, X. Zhou and G. Cui, *Small*, 2018, 14, 1–16.

49 P.-J. Alarco, Y. Abu-Lebdeh, A. Abouimrane and M. Armand, *Nat. Mater.*, 2004, 3, 476.

50 R. Khurana, J. L. Schaefer, L. A. Archer and G. W. Coates, *J. Am. Chem. Soc.*, 2014, 136, 7395–7402.

51 A. Mahmoud, J. M. Amarilla and I. Saadoune, *Electrochim. Acta*, 2015, 163, 213–222.

Published in : Journal of Materials Chemistry A (2019), vol. 7, issue 16, pp. 9844-9853
doi.org/10.1039/c9ta01564g
Status : Postprint (Author's version)

52 Y. Yin, M. Gao, H. Pan, L. Shen, X. Ye, Y. Liu, P. S. Fedkiw and X. Zhang, *J. Power Sources*, 2012, 199, 256–262.

53 C. S. Kim and S. M. Oh, *Electrochim. Acta*, 2001, 46, 1323– 1331.

54 R. C. Agrawal and G. P. Pandey, *J. Phys. D: Appl. Phys*., 2008, 41, 223001.

55 Z. Huang, Q. Pan, D. M. Smith and C. Y. Li, *Adv. Mater. Interfaces*, 2019, 6, 1801445.

56 G. Fu and T. Kyu, *Langmuir*, 2017, 33, 13973–13981.

57 H. Yue, J. Li, Q. Wang, C. Li, J. Zhang, Q. Li, X. Li, H. Zhang and S. Yang, *ACS Sustainable Chem. Eng*., 2018, 6, 268–274.

58 G. Fu, J. Dempsey, K. Izaki, K. Adachi, Y. Tsukahara and T. Kyu, *J. Power Sources*, 2017, 359, 441–449.

59 K. Kimura, M. Yajima and Y. Tominaga, *Electrochem. Commun*., 2016, 66, 46–48.

60 S. Dabral and T. Schaub, *Adv. Synth. Catal.*, 2019, 361, 223– 246.